Chinese Chemical Letters 35 (2024) 109788

Contents lists available at ScienceDirect

Chinese Chemical Letters

journal homepage: www.elsevier.com/locate/cclet

Vacuum promoted on-tissue derivatization strategy: Unravelling spatial distribution of glycerides on tissue

Yu-Qi Cao[a,b,1], Ying-Jie Lu[a,c,1], Li Zhang[a], Jing Zhang[a,*], Yin-Long Guo[a,*]

[a] State Key Laboratory of Organometallic Chemistry and National Center for Organic Mass Spectrometry in Shanghai, Center for Excellence in Molecular Synthesis, Shanghai Institute of Organic Chemistry, University of Chinese Academy of Sciences, Chinese Academy of Sciences, Shanghai 200032, China
[b] Technical Centre, Shanghai Tobacco (Group) Corp., Shanghai 200082, China
[c] Department of Pharmacognosy, School of Pharmacy, Naval Medical University, Shanghai 200433, China

ARTICLE INFO

Article history:
Received 3 December 2023
Revised 19 February 2024
Accepted 18 March 2024
Available online 19 March 2024

Keywords:
Mass spectrometry imaging
On-tissue derivatization
Glycerides
Alzheimer's disease

ABSTRACT

Matrix-assisted laser desorption ionization-mass spectrometry imaging (MALDI-MSI) has shown its capability in visualizing the spatial distribution of various kinds of endogenous metabolites. Nevertheless, high quality mass imaging of low polar metabolites remains challenging. Herein, a platform for sensitive matrix-assisted laser desorption ionization-mass spectrometry imaging of cholesterol and glycerides has been proposed. In the platform, a vacuum promoted on-tissue derivatization strategy was proposed to constantly make the derivatization reaction proceed towards to the direction of products. Compared with traditional on-tissue derivatization procedure, the strategy improved the acquired intensity of derivatized glycerides about 50%. Additionally, the mass spectrometry image reflecting the signal ratio between 3 classes of glycerides was achieved to exploit the metabolic level of glycerides on tissue slice. Finally, the platform was applied to brain slices of Alzheimer's transgenic mice, type 2 diabetes mice and normal mice. Significant difference was found in mass spectrometry images reflecting the signal ratio of multiple endogenous metabolites. The work constructed a promising platform for mapping of glycerides in tissue by mass spectrometry imaging.

Glycerides are typical low polar metabolites with multiple biological functions and play important roles in numerous diseases [1]. Glycerides existing in tissue could be split into 3 classes including triacylglycerols (TAGs), diacylglycerols (DAGs), monoacylglycerols (MAGs). The level of TAGs has been recognized as a reliable biomarker for diagnosis of diseases [2]. DAGs have been widely recognized as second messengers in cell signal transduction [3,4]. MAGs could be degraded to produce free fatty acids and glycerol through MAG lipases [5]. Therefore, unravelling the spatial distribution and abundance of glyceride in tissues may promote the understanding of glycerides metabolism process and the diagnosis of diseases.

Mass spectrometry imaging (MSI) is a molecular imaging technique with advantages of no-labelling and *in-situ*. In the field of MSI, vacuum MSI and ambient MSI are two mainly techniques according to the detection environment. When it comes to analyzing glycerides, Cai's group successfully showed that atmospheric pressure-MALDI-MSI (AP-MALDI-MSI) could visualized a series classes of lipids including TAGs *via* optimized matrix 2,5-dihydroxyacetophenone [6]. AP-MALDI-MSI combined with enzymatic degradation realized the visualization of TAG and DAGs on textile surface [7]. Our group developed an online quaternized derivatization method combined with laser ablation carbon fiber ionization-MSI for imaging MAGs and DAGs [8]. In addition, direct analysis in real time has been found possess sensitivity to low polar lipids [9]. However, imaging under atmospheric environment would greatly decrease the detection sensitivity of target analytes. Vacuum MSI represented by Matrix-assisted laser/desorption ionization-MSI (MALDI-MSI) has shown its ability in imaging endogenous lipids containing partial glycerides with optimized matrix dithranol [10,11]. Although MALDI-MSI can ensure the detection sensitivity and spatial resolution, there still lacks a systematic imaging strategy for three classes of glycerides by MALDI-MSI. Moreover, spatial localization of low polar metabolites by MALDI remains a challenge [12–20]. Typically, various endogenous metabolites are ionized simultaneously after laser irradiation in MALDI-MSI. Metabolites with high polarity like phospholipids seem to enjoy greater ionization efficiency than low polar metabolites [12,20], seriously obstructing the detection of low polar metabolites like cholesterols and glycerides. Hence, it is imper-

* Corresponding authors.
E-mail addresses: zhangjing@sioc.ac.cn (J. Zhang), ylguo@sioc.ac.cn (Y.-L. Guo).
[1] These authors contributed equally to this work.

https://doi.org/10.1016/j.cclet.2024.109788
1001-8417/

ative to propose a tissue preprocessing strategy to unravel the spatial localization of glycerides by MALDI-MSI.

Up to now, sample preprocessing methods like on-tissue modification has been developed to improve the mass signal of target compounds in MALDI-MSI. For example, metal cationization laser desorption/ionization utilized an optimized concentration of metal ion salt applied on tissue sample to improve the detective sensitivity of analytes [14]. Prof. Caprioli's group have pointed out that the mass signals of TAGs may be improved drastically in MALDI-MSI after spraying sodium salt solution [21]. Besides metal cationization, on-tissue derivatization also attracts interests of many researchers. On-tissue derivatization targets a specific chemical group by applying a derivatization reagent that chemically reacts on tissue. Then the mass intensity of target compounds in MALDI-MSI can be enhanced [22]. Girard's Reagent is a reagent targeting carbonyl group for derivatizing low-polarity steroid metabolites [23–26]. In 2022, Prof. Xiao Wan's group reported novel on-tissue cycloaddition reagent for MALDI-MSI of lipid C=C position isomers [27]. The development of these specially designed derivatization reaction has substantially expanded the range of ionizable metabolites in MALDI-MSI. However, it remains a challenge to propose a reliable on-tissue modification method that could significantly improve the mass signal of glycerides in MALDI-MSI.

Herein, inspired by previous works [28–31], a platform for sensitive MALDI-MSI of glycerides has been developed. On-tissue derivatization of cholesterol, MAGs and DAGs was performed on one tissue slice with assistance of *N*-alkyl pyridinium quaternization reaction [29–32]. Remarkably, unique from traditional sample preprocessing protocols, a vacuum promoted on-tissue derivatization strategy was proposed here to help improve reaction efficiency. Owing to vacuum promoted strategy, the acquired intensity of derivatized glycerides improved about 50%. After the derivatization reaction, a couple of mass tags with 5 Da difference would be added to endogenous metabolites containing hydroxyl group, which may offer great convenience for identification [31,32]. Meanwhile, an adjacent tissue slice was used for MSI of TAGs. Due to lack of hydroxyl group in TAGs, an optimized concentration of sodium salt was sprayed onto the tissue to form the sodium adducts of TAGs [21]. Then, the two adjacent tissue slices were simultaneously sent into MALDI to perform MSI experiments. The developed method here was applied to brain slices of normal mice and Alzheimer's transgenic mice, significant difference was found in MS images reflecting the signal ratio of multiple endogenous metabolites. To summarize, a comprehensive platform for MS imaging of glycerides has been constructed here, which may offer new inspirations for the analysis of low polar endogenous metabolites.

In MALDI-MSI, the tissue slices would be directly sent into the mass spectrometer after matrix spraying. Such practice provides us with abundant information about metabolites of high abundance and polarity like phospholipids, neurotransmitters, free fatty acids and *etc*. However, such practice seems to be unsuitable for neutral lipids like glycerides due to compromised ionization efficiency in MALDI. On-tissue derivatization has been proposed to dramatically improve the detecting sensitivity of these metabolites. As previously discussed, glycerides are consisted of MAGs, DAGs and TAGs. These three classes of glycerides all share a same chemical skeleton while their side chains differ from each other. In MAGs and DAGs, just one or two hydroxyl groups in glycerol have been substituted to form ester bonds. The application of an on-tissue derivatization method targeting hydroxyl group may remove obstacles in the detection of MAGs and DAGs. On the contrary, TAGs consist none hydroxyl groups, making it difficult to target a typical chemical group for on-tissue derivatization in three classes of glycerides. Consequently, metal cationization laser desorption/ionization was adopted for MSI of TAGs. TAGs have greater inclination to form adduct with sodium ion as compared with proton [33,34].

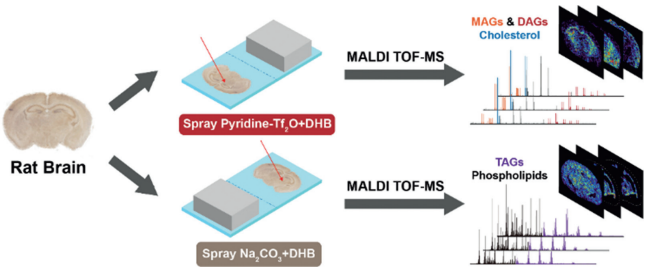

Fig. 1. Configuration of the platform for MALDI-MSI of glycerides.

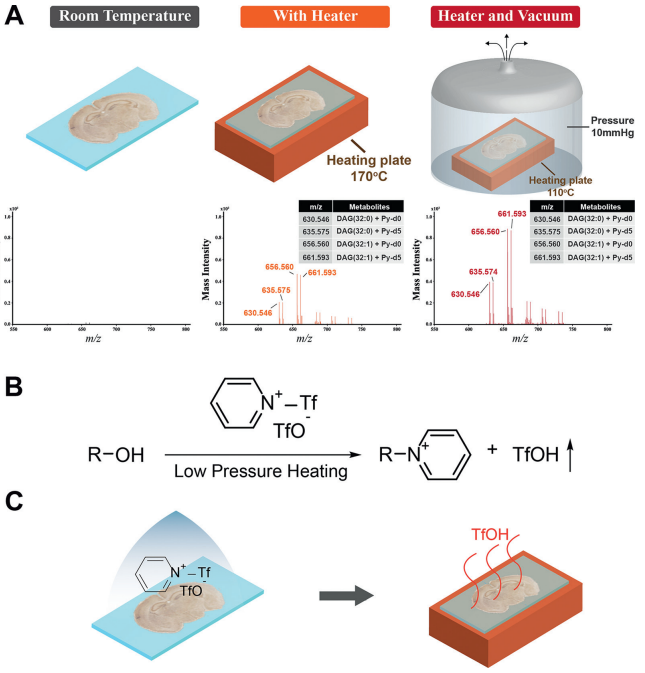

Fig. 2. (A) The comparison of acquired mass signal of DAG(32:0) under 3 different sample preprocessing procedures after spraying derivatization reagents. (B) Chemical equation of the vacuum promoted *N*-alkyl pyridinium quaternization reaction. (C) Schematic image about the evaporation of TfOH with heater.

According to the above proposal for improving detection sensitivity of glycerides, a platform for comprehensive MALDI-MSI of glycerides could be developed here. As shown in Fig. 1, two consecutive sections are mounted onto a glass slide and sent into the instrument for MALDI-MSI simultaneously. One slice undertakes the MSI task of MAGs and DAGs as the other one is responsible for MSI of TAGs.

N-Alkyl pyridinium quaternization reaction has become an efficient derivatization reaction for MS analysis of free fatty alcohols and sterols in biological samples [29–32]. The main chemical reagents used in *N*-alkyl pyridinium quaternization reaction include a couple of isotopic labelling reagents: pyridine-d_0, pyridine-d_5 and trifluoromethanesulfonic anhydride (Tf_2O). With the assistance of Tf_2O, pyridine could rapidly substitute the hydroxyl groups in compounds and a quaternized pyridine would be added into the compounds (Fig. 2B). As the quaternized pyridine group contains a positive charge itself, the derivatized product is endowed with great ionization efficiency in MS. Remarkably, the positive charge originates from the reaction process but not the reacting reagents, which is unique as most other derivatization reactions applies quaternary ammonium salt containing positive charge itself. What is more, the application of a couple of isotopic la-

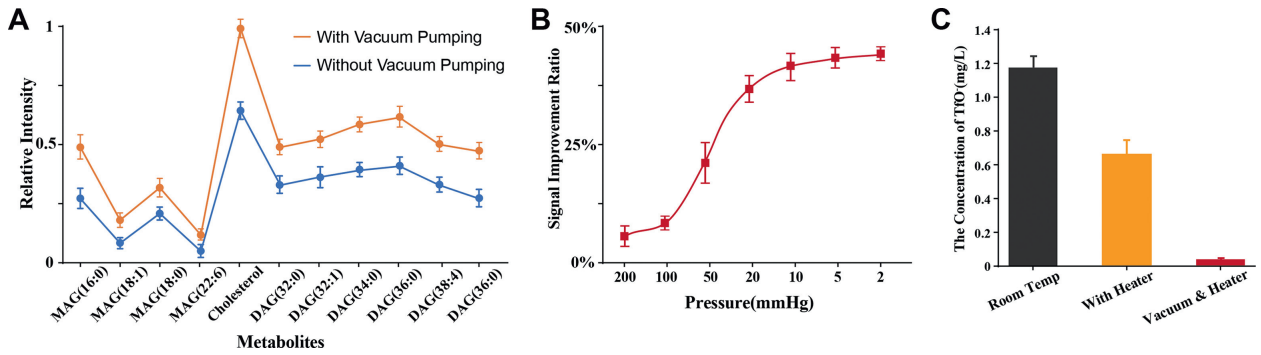

Fig. 3. (A) Comparison of acquired mass intensity with and without vacuum pumping. (B) The mass signal improvement ratio *vs* pressure in airtight container (DAG(32:0) as reference). (C) Measured concentration of TfO^- on tissue surface under 3 experimental conditions.

belling reagents: pyridine-d_0, pyridine-d_5 is of great benefit for the identification of derivatized products. For each derivatized alcohol, a pair of mass peaks with a *m/z* difference of 5.032 Da emerges in the acquired MS spectra.

However, the *N*-alkyl pyridinium quaternization reaction cannot be directly applied for on-tissue derivatization. In our pioneering attempts, we intended to spray pyridinium and Tf_2O onto tissue respectively (not in liquid mixture). The tissue surface became sticky after spraying pyridine and serious analyte delocalization phenomenon was observed due to pyridine is an oil-like liquid. A solution was then figured out that pyridinium and Tf_2O was premixed to form a new pyridinium salt. The pyridinium salt could form an even thin film on tissue slice using a homemade derivatization reagent spraying apparatus (Figs. S1 and S2 in Supporting information). At the early stage, the matrix was immediately sprayed onto tissue slice after the thin pyridinium salt film formed. Unfortunately, no mass signal related to glycerides was captured, which might attribute to the stable situation of sprayed pyridinium salt in room temperature and TfOH would be generated. TfOH has a comparatively high boiling point that it is hard for TfOH to get away from the tissue slice surface in room temperature. The existence of TfOH may obstruct the reaction proceed towards the product direction. Based on the above analysis, the tissue slice was placed onto a heater with 170 °C after spraying derivatization reagent. The high temperature may result in the decomposition of pyridinium salt, extraction of pyridinine and evaporation of generated TfOH (Fig. 2C). Then, the mass signals of multiple MAGs and DAGs were captured. However, such high temperature may lead to side effect. The information of many valuable metabolites may lose during the heating process. On the other side, heating process may cause serious diffusion of analytes, which would significantly reduce spatial resolution. To fix the problem, a novel on-tissue derivatization strategy named as vacuum promoted derivatization was then proposed. Vacuum may reduce the boiling point of reaction by-products. In the *N*-alkyl pyridinium reaction, the boiling point of reaction by-product TfOH was significantly reduced under environment with reduced pressure, which may promote the derivatization reaction towards direction of products. As shown in Fig. 2A, the tissue slice and heating plate was placed into an airtight container. Then, the pressure inner the container rapidly decreased with assistance of an oil pump. The temperature of the heating plate was controlled about 110 °C. According to the chemical equation shown in Fig. 2B, the reaction may proceed smoothly with comparatively low resistance. As shown in Fig. 3A, the mass signals of derivatized MAGs and DAGs evidently improved about 50%. The parameter optimization experiment was performed later to determine the optimal air pressure for derivatization. The mass signal increased rapidly as the air pressure inner container dropped. The mass signal became stable when the air pressure was lower than 5 mmHg (Fig. 3B).

To explore mechanism beneath the signal enhancement phenomenon, we assumed that vacuum may assist the evaporation of TfOH. As shown in Fig. 3C, the concentration of TfO^- on surface of the tissue slice was measured (Figs. S4-S6 in Supporting information). The result showed that the addition of vacuum greatly decreased the concentration of TfO^- on tissue slice. As discussed previously, the continuous removal of TfOH may promote the derivatization reaction towards product direction.

Three chemicals belonging to MAGs, DAGs and cholesterol were selected to perform the validation experiment of the on-tissue derivatization method. As displayed in Fig. S7A (Supporting information), the mass signals of derivatized MAG(18:1), cholesterol and DAG(32:1) were captured with high intensity in the acquired MALDI spectra. For each chemical, both derivatized products generated from reaction with pyridine-d_0 and pyridine-d_5 emerged as a pair of mass peaks with similar mass intensity, which extremely simplify the identification process. Taking cholesterol as an example, the *m/z* 448.394 and *m/z* 453.426 correspond to derivatized cholesterol and *m/z* 369.352 corresponds to underivatized cholesterol. The mass signals of derivatized products were far higher than underivatized one, inferring the drastic improvement of detecting sensitivity. Also, protonated pyridine-d_0 and pyridine-d_5 were produced as representative ions in MS^2 spectra of the three chemicals, which may add solid proof for identification of metabolites (Fig. S7C in Supporting information). Furthermore, MALDI-MSI experiment of derivatives of MAG(18:1) with gradient concentration has been performed. As illustrated in Fig. S7B (Supporting information), the integral mass intensity gradually increased as the concentrations of MAG(18:1) increased. To summarize, an on-tissue derivatization workflow targeting hydroxyl group has been constructed here.

After construction of the platform for on-tissue derivatization and sodium salt spraying, the platform was then applied to the brain tissue slices of mice. Comparison of the acquired average mass spectra with and without the platform were demonstrated in Fig. 4. In Fig. 4A, the above referred to mass spectrum after on-tissue derivatization while the bottom was mass spectrum acquired using tissue slice sprayed matrix directly. In *m/z* 350–800, multiple pairs of mass peaks with *m/z* difference of 5.032 Da emerged in the above mass spectrum. After accurate mass calculation of the acquired mass peaks, the mass signals of 4 derivatized MAGs, derivatized cholesterol and 6 derivatized DAGs were confirmed. The detailed information of the 11 derivatized endogenous metabolites are listed in Table S1 (Supporting information). On the contrary, in *m/z* 350–700, most no valuable mass peak was captured in the bottom mass spectrum. Only the mass signals of several phospholipids were captured in *m/z* 700–800. As previously discussed, phospholipids are of high polarity, which endows them with excellent detecting sensitivity in MALDI. Due to the high abundance of phospholipids, they could result in serious ion

suppression effect to other endogenous species without on-tissue derivatization. The ionization of neutral lipids like cholesterol, MAGs and DAGs are almost completely suppressed due to their comparatively low affinity to H^+ ion and low abundance. As the derivatization reagent rapidly reacted with endogenous MAGs, cholesterol and DAGs, the polarity of the derivatized products has gone through a sharp increase. These endogenous species have been added with a quaternized pyridine group and then enjoyed high priority during the ionization process of MALDI. Simply speaking, the polarity balance between phospholipids and glycerides has been broken and the ionization of derivatized cholesterol, MAGs and DAGs may no longer be disturbed by phospholipids.

The acquired mass spectrum after sodium salt spraying is shown in Fig. 4B. As illustrated, the purple mass peaks represent the captured mass signals of TAGs and the black mass peaks belong to phospholipids. Several sodium salt doping parameters were optimized, including the type of sodium salt, spraying volume, and ESI sprayer distance. Detailed optimization information could be found in Fig. S8 (Supporting information). After sodium salt spraying under the optimal condition, a great many mass signals identified as sodium adducts of TAGs emerge in the spectrum. Such result is corresponding to the research progress reported previously [14,21]. As TAGs have inclination to form sodium adduct ions, the addition of adequate concentration of sodium salt solution evidently improves the detection sensitivity of TAGs. Finally, 12 TAGs have been identified from the MALDI mass spectra and detailed information about the identified TAGs in tissue slice could be found in Table S2 (Supporting information).

Fig. 5 illustrates the acquired MS images belonging to cholesterol and 16 different glycerides. As illustrated in MS image of cholesterol, the mass intensity of cholesterol is significantly higher in white matter region then grey matter region, which complied with previous study [35]. The MS images of different MAGs and DAGs possessed great similarity inside their lipid classes. Meanwhile, the spatial distribution of most MAGs showed evident difference with that of DAGs. For example, as reflected by MS image of ion with *m/z* 392.316, MAG(16:0) mainly existed in brain's striatum zone and had comparatively low signal intensity in the cortex region of brain. On the contrary, the mass signal of DAG(32:0) was hard to be captured in the striatum region of mice brain while the cortex zone of mice brain contained higher amount of DAG(32:0). Such phenomenon unraveled the different spatial distribution of MAGs and DAGs in mice brain slice, which may indicate that MAGs and DAGs undertake unique biological functions in mammals, respectively. When it comes to TAGs, the circumstance became a little bit complicated. The spatial distribution of some kinds of TAGs showed similar trends with that of most MAGs. However, the other kinds of TAGs possessed similar spatial distribution with most DAGs. In a word, the platform constructed here provides us with a comprehensive portrait reflecting the spatial distribution of cholesterol and glycerides on tissue slice, which may offer assistance for understanding the biological value of these endogenous metabolites.

According to various research, the three classes of glycerides including MAGs, DAGs and TAGs are crucial components in lipid metabolism. Also, MAGs and DAGs are mainly produced through the enzymatic degradation of TAGs. As a result, monitoring one single metabolite may not accurately reflect the metabolism of glycerides. On the other side, the activity of enzyme relating to glyceride metabolism could be precisely exhibited through analyzing the signal ratio between different classes of glycerides. As two adjacent tissue slices were used in the developed platform for acquiring MS images of MAGs, DAGs and TAGs respectively, the ratio MS images between MAGs, DAGs and TAGs could not be readily achieved through one-step calculation. Consequently, a method for resolving the metabolic information from two adjacent tissue slices have to be proposed here.

Fig. 6 shows the workflow of calculating method for acquirement of ratio MS images. Firstly, a glass slide with two adjacent tissue slices went through on-tissue derivatization, sodium salt

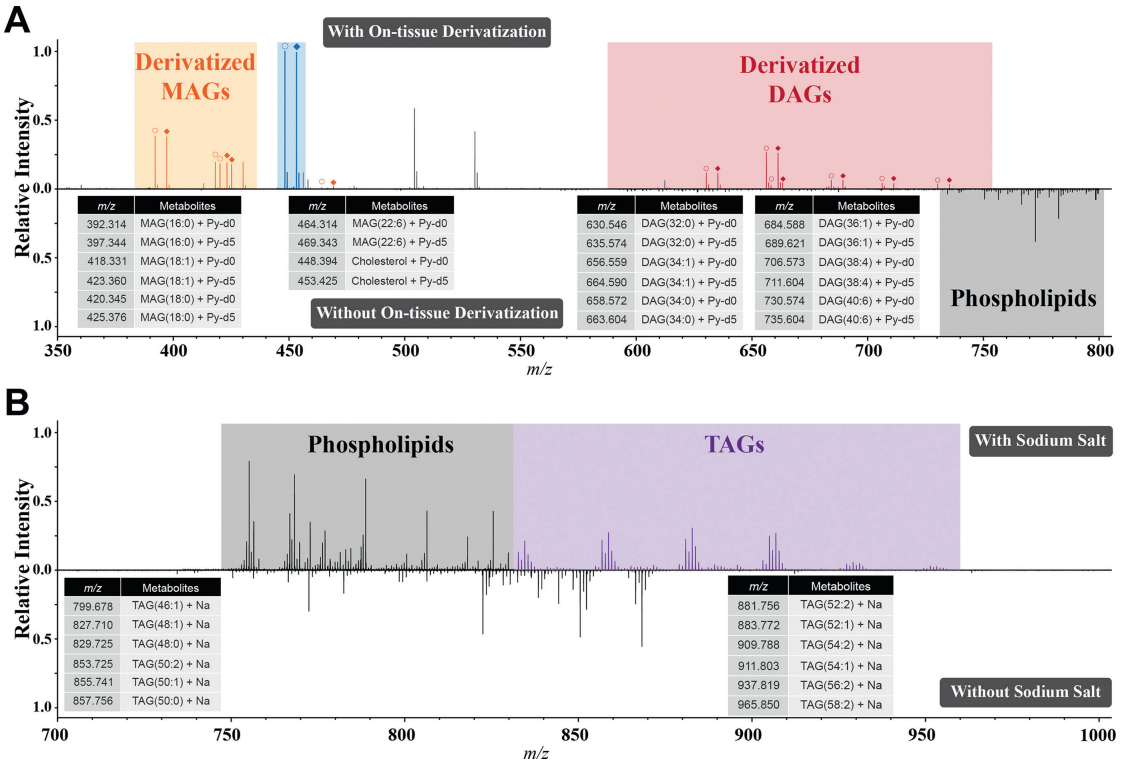

Fig. 4. (A) Comparison of the acquired mass spectra before and after on-tissue derivatization. (B) Comparison of the acquired mass spectra with and without sodium salt solution spraying.

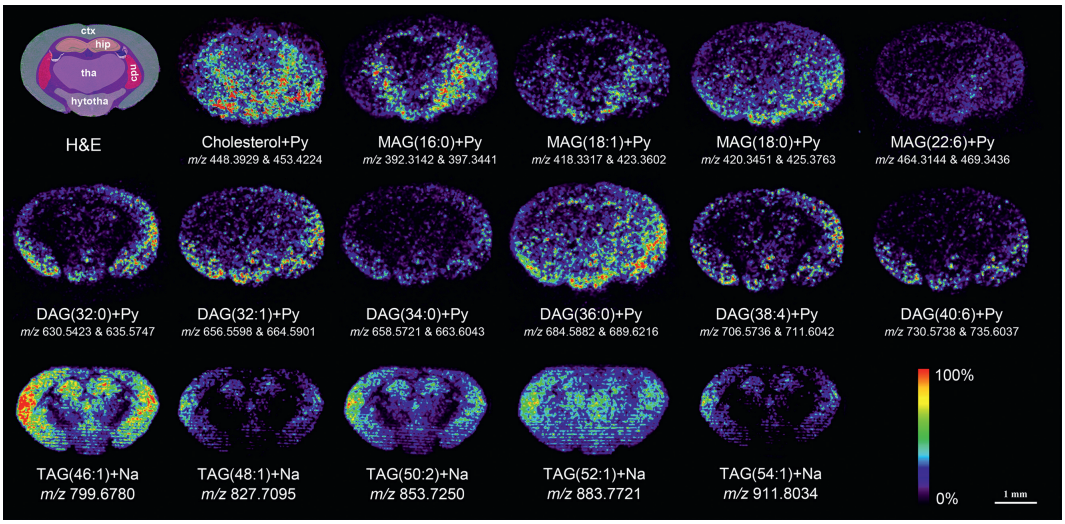

Fig. 5. Acquired MS images of cholesterol and glycerides using the new MALDI-MSI platform. Ctx, cerebral cortex; Hip, hippocampus; Cpu, caudate putamen; hypotha, hypothalamus; tha, thalamus.

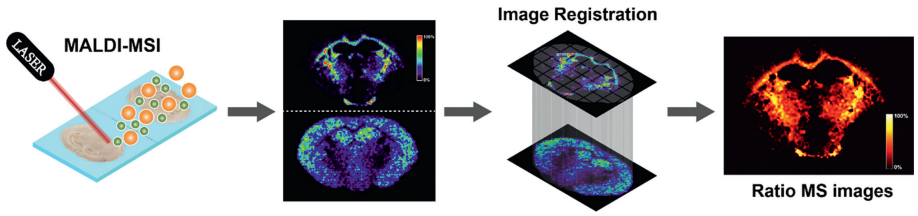

Fig. 6. Workflow of the Generation of MS images reflecting the signal ratio between different classes of species.

spraying and matrix applying as previously discussed. Then, the glass slide was sent into the MALDI-TOF-MS instrument to perform MSI experiment. As every glyceride has a specific *m/z* value, the MS image of two kinds of glycerides cannot be acquired through extracting a single *m/z* value directly. Thus, a homemade software was programmed to integrate the MS images belonging to two different *m/z* values. To calculate the intensity ratio of every pixel in the two pieces, an image co-registration program was created to align the MS image data of the two pieces in pixel level. Information about the user interface and the algorithm of the homemade software could be found in Figs. S10-S17 (Supporting information). The home-made software for MSI image registration was powered by a series of open-source Python package and has not been previously reported. The software has been granted the software copyright, with the registration Nos. 2020SR0721725 & 2020SR0721918. Owing to highly resemblance and simultaneously imaging of two adjacent slices, one slice could coincide with the other one through moving, folding and rotating transformations. Dice-Sorenson coefficient was used to determine if optimal coincidence was achieved. The Dice-Sorenson coefficient was 0.82 ($\pm$0.3) for all the MS image pairs (Fig. S18 and Table S5 in Supporting information), indicating that two derivatized slices as registered can be expected to achieve over 80% overlap. Thus, region registration between the two pieces was realized. With the application of the program, new MS images reflecting the signal ratio between different classes of species could be readily achieved. These MS images are of great benefit for deeper investigation of cholesterol and glyceride metabolism.

Currently, millions of people worldwide have been afflicted by Alzheimer's disease and type 2 diabetes mellitus. According to various research [36–40], the disorder in metabolism of cholesterol and glycerides exists in both Alzheimer's disease and type 2 diabetes. Whether the two diseases share a common etiology mechanism has become a research hotspot. Here, as the platform constructed here could unravel the spatial distribution of glycerides in tissue slices, we hope to find out whether the metabolism of the glycerides in mice with the two diseases respectively have the same changing trend as compared with normal mice.

The brains of Alzheimer's transgenic mice and diabetes mellitus mice were frozen and sliced as experimental samples. The brain tissue slices of normal mice were prepared as controlled samples. Taking advantage of the constructed platform, the ratio MS images of different classes of glycerides could be readily acquired. As shown in Fig. 7A, representative ratio MS images were acquired to uncover the metabolic difference of glycerides between normal mice and Alzheimer's transgenic mice. The left half part of the brain MS image represented normal mice while the right half part represented Alzheimer's transgenic mice. Obviously, the ratio intensity of MAG and DAG to TAG seemed to be higher in Alzheimer's transgenic mice as compared with normal mice. To confirm the experimental result, we performed additional experiments with homogenate of mice brain tissue. The experimental results using brain tissue homogenate (Table S6 in Supporting information) also supported the observation from MALDI-MSI that the ratio intensity of MAG and DAG to TAG seemed to be higher in Alzheimer's transgenic mice as compared with normal mice. Such phenomenon may infer that the metabolism of glycerides is more active in Alzheimer's transgenic mice as more MAGs and DAGs are produced through the enzymatic degradation of TAGs. Also, the representative ratio MS images which unravel the metabolic difference of glycerides between normal mice and type 2 diabetes mice could be found in Fig. 7A. The changing trend of the glycerides metabolic level reflected by these images seemed to be similar with that of Alzheimer's transgenic mice. On the other side, systematic error still exists in the above approach comparing the changing trend of the glycerides metabolic level in type 2 diabetes mice and Alzheimer's transgenic mice. Frankly speaking, the reac-

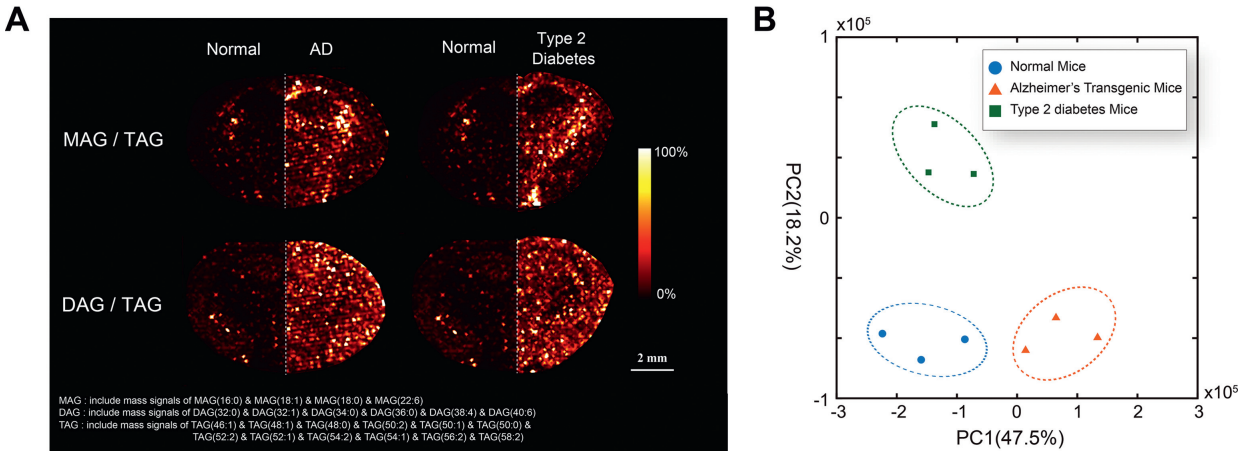

Fig. 7. (A) Comparison of the acquired ratio MS images from brain slice of Alzheimer's mice and Type 2 diabetes mice. (B) PCA plot of tissue slices from normal mice, Alzheimer's transgenic mice and Type 2 diabetes mice.

tion efficiency and deposition way of sodium bicarb would produce systematic error for the generated ratio MS images. A more accurate evaluation tool is still under investigation. Furthermore, the average intensity of all imaged glycerides and cholesterol was calculated and normalized to perform the principal component analysis (PCA). The first (47.5%) and the second (18.2%) components were chosen to analyze the entry gate, tissue slice sample in the PCA plot. As shown, the three kinds of tissues were readily separated (Fig. 7B). To summarize, the MS signal changing trend of glycerides achieved using the platform may offer some inspiration for investigating the connection between Alzheimer's disease and type 2 diabetes. The MS images and ratio MS images of parallel experiments are shown in Figs. S19-S28 (Supporting information).

In summary, the work demonstrated a platform for sensitive MALDI-MSI of glycerides. Owing to the application of vacuum Promoted On-tissue derivatization strategy, the MS images of cholesterol, MAGs and DAGs could be readily acquired. After *N*-alkyl pyridinium quaternization reaction, a couple of charged mass tags with 5 Da *m/z* difference would be added to endogenous metabolites containing hydroxyl group, which drastically increase the ionization efficiency and may offer great convenience for identification of derivatized metabolites. Also, an adjacent tissue slice was sprayed sodium solution to perform the MALDI-MSI of TAGs simultaneously. After MSI experiment, the ratio MS images reflecting the signal ratio between 3 classes of glycerides were generated through specially designed programs. The platform also uncovered the metabolic difference of cholesterol and glycerides between brain tissue slices from normal mice, Alzheimer's transgenic mice and type 2 diabetes mice. We anticipate that the platform proposed here would be crucial complement for MALDI-MSI sample pretreatment and on-tissue derivatization studies. In addition, the platform may promote investigation on the identification of new glycerides on various kinds of tissues.

Declaration of competing interest

The authors declare that they have no known competing financial interests or personal relationships that could have appeared to influence the work reported in this paper.

CRediT authorship contribution statement

Yu-Qi Cao: Data curation, Investigation, Methodology, Writing – original draft. **Ying-Jie Lu:** Investigation, Methodology, Writing – original draft. **Li Zhang:** Methodology, Validation. **Jing Zhang:** Investigation, Validation, Writing – review & editing. **Yin-Long Guo:** Conceptualization, Funding acquisition, Methodology, Writing – review & editing.

Acknowledgments

This work was supported by the National Key R & D Program of China (No. 2021YFF0701900), the Strategic Priority Research Program of the Chinese Academy of Sciences (No. XDB0610000), Shanghai Science and Technology Innovation Action Plan (No. 21142200800), and the Program of EnShi TuJia & Miao Autonomous Prefecture Bureau of Scientific & Technological Affairs.

Supplementary materials

Supplementary material associated with this article can be found, in the online version, at doi:10.1016/j.cclet.2024.109788.

References

[1] M.J. Chapman, H.N. Ginsberg, P. Amarenco, et al., Eur. Heart. J. 32 (2011) 1345–1361.
[2] C.L.E. Yen, S.J. Stone, S. Koliwad, et al., J. Lipid. Res. 49 (2008) 2283–2301.
[3] D.M. Erion, G.I. Shulman, Nat. Med. 16 (2010) 400–402.
[4] F. Colón-González, M.G. Kazanietz, Biochim. Biophys. Acta 1761 (2006) 827–837.
[5] X. Luo, C. Cheng, Z. Tan, et al., Mol. Cancer 16 (2017) 76.
[6] T. Zeng, R. Zhang, Y. Chen, et al., Talanta 245 (2022) 123466.
[7] J. Hall-Andersen, S.G. Kaasgaard, C. Janfelt, Chem. Phys. Lipids 211 (2018) 100–106.
[8] Y. Lu, Y. Cao, L. Zhang, et al., Anal. Chem. 94 (2022) 3756–3761.
[9] R.B. Cody, A.J. Dane, J. Am. Soc. Mass Spectrom. 24 (2013) 329–334.
[10] C.H. Le, J. Han, C.H. Borchers, Anal. Chem. 84 (2012) 8391–8398.
[11] J. Chen, P. Xie, P. Wu, et al., Chin. Chem. Lett. 35 (2024) 108895.
[12] J.A. Fincher, D.R. Jones, A.R. Korte, et al., Sci. Rep. 9 (2019) 17508.
[13] J. Son, G. Lee, S. Cha, J. Am. Soc. Mass Spectrom. 25 (2014) 891–894.
[14] M. Dufresne, J.F. Masson, P. Chaurand, Anal. Chem. 88 (2016) 6018–6025.
[15] S.N. Jackson, K. Baldwin, L. Muller, et al., Anal. Bioanal. Chem. 406 (2014) 1377–1386.
[16] C. Liu, K. Qi, L. Yao, et al., Anal. Chem. 91 (2019) 6616–6623.
[17] J. Soltwisch, B. Heijs, A. Koch, et al., Anal. Chem. 92 (2020) 8697–8703.
[18] J. Soltwisch, H. Kettling, S. Vens-Cappell, et al., Science 348 (2015) 211.
[19] A. Knodel, D. Foest, S. Brandt, et al., Anal. Chem. 92 (2020) 15212–15220.
[20] M.S. Boskamp, J. Soltwisch, Anal. Chem. 92 (2020) 5222–5230.
[21] M. Dufresne, N.H. Patterson, J.L. Norris, R.M. Caprioli, Anal. Chem. 91 (2019) 12928–12934.
[22] C. Harkin, K.W. Smith, F.L. Cruickshank, et al., Mass Spectrom. Rev. 41 (2022) 662–694.
[23] E. Takeo, Y. Sugiura, T. Uemura, et al., Anal. Chem. 91 (2019) 8918–8925.
[24] D.F. Cobice, C.L. Mackay, R.J.A. Goodwin, et al., Anal. Chem. 85 (2013) 11576–11584.
[25] D.F. Cobice, D.E.W. Livingstone, C.L. Mackay, et al., Anal. Chem. 88 (2016) 10362–10367.
[26] F.P.Y. Barré, B. Flinders, J.P. Garcia, et al., Anal. Chem. 88 (2016) 12051–12059.
[27] W. Daijie, L. Lili, H. Yuhao, et al., Chin. Chem. Lett. 33 (2022) 2073–2076.

[28] S.S. Wang, Y.J. Wang, J. Zhang, et al., Anal. Chem. 91 (2019) 4070–4076.
[29] H. Wang, H. Wang, L. Zhang, et al., Anal. Chim. Acta 690 (2011) 1–9.
[30] Y. Cao, Q. Guan, T. Sun, et al., Anal. Chim. Acta 937 (2016) 80–86.
[31] Y.Q. Cao, L. Zhang, J. Zhang, Y.L. Guo, Anal. Chem. 92 (2020) 8378–8385.
[32] W. Qi, Y. Wang, Y. Cao, et al., Anal. Chem. 92 (2020) 8644–8648.
[33] E. Pittenauer, G. Allmaier, J. Am. Soc. Mass Spectrom. 20 (2009) 1037–1047.
[34] G. Picariello, A. Paduano, R. Sacchi, F. Addeo, J. Agric. Food Chem. 57 (2009) 5391–5400.
[35] M. Dufresne, A. Thomas, J. Breault-Turcot, et al., Anal. Chem. 85 (2013) 3318–3324.
[36] L. Puglielli, R.E. Tanzi, D.M. Kovacs, Nat. Neurosci. 6 (2003) 345–351.
[37] X. Zhang, W. Liu, J. Zan, et al., Sci. Rep. 10 (2020) 14509.
[38] X. Han, Curr. Alzheimer Res. 2 (2005) 65–77.
[39] H. Sone, H. Ito, Y. Ohashi, et al., The Lancet 361 (2003) 85.
[40] V.A. Diwadkar, J.W. Anderson, S.R. Bridges, et al., Proc. Soc. Exp. Biol. Med. 222 (1999) 178–184.